VILNIUS TECH
Vilnius Gediminas Technical University

Journal of Environmental Engineering and Landscape Management
ISSN 1648–6897 / eISSN 1822-4199
2022 Volume 30 Issue 2: 308–320
https://doi.org/10.3846/jeelm.2022.16747

Special issue on *Sustainable Environmental Processes and Technologies*

GREEN SYNTHESIS OF IRON-OXIDE NANOPARTICLES USING SCRAP IRON AS PRECURSOR FOR THE REMOVAL OF PB (II) FROM AQUEOUS MEDIUM

Mohd TAQUI[1], Sneha DAS[2*], Tuhin KAMILYA[3], Sandip MONDAL[4], Surabhi CHAUDHURI[5]

[1, 2, 3, 4]*Department of Earth and Environmental Studies, NIT Durgapur, 713209 West Bengal, India*
[5]*Department of Bio-Technology, NIT Durgapur, 713209 West Bengal, India*

Received 15 January 2021; accepted 22 September 2021

Highlights

- Green synthesis of iron-based nanoparticles using scrap iron (waste material) and pomegranate peel extract as a reducing agent.
- This method has many advantages as it can be synthesized in a very short period, low cost of production, environmentally friendly, and easy as single-step reaction is required for the synthesis of iron oxide nanoparticle.
- The sorption mechanism follows the Langmuir isotherm model and the reaction rate best fitted by pseudo second order model.

Abstract. In the present study, low-cost, environmentally friendly, single-step, high productive novel Iron-oxide nanoparticles (NPs) were prepared from scrap iron using a green synthesis method to remove Pb (II) from aqueous solution. The characterization of synthesized nanoparticles was conducted by UV-vis spectroscopy. The crystalline structure and the phase change were clarified by XRD. FE-SEM was done to know the morphology of iron oxide nanoparticles, and the average surface area of 46.856 m^2/g was found by the BET surface area analyzer. The XRD plot shows that the obtained magnetite Fe_3O_4 combines FeO and Fe_2O_3 as the synthesis was conducted in the open atmosphere. The SEM images confirm the formation of iron oxide nanoparticles with a size of 31 nm. The removal efficiency of the adsorbent was carried out by optimizing the different operational parameters like pH, time, adsorbent dosage, initial concentration of metal ion, contact time by batch studies. The obtained pHzpc (pH 5.7) value indicates that the adsorption process will be favorable at higher pH. The maximum removal efficiency and uptake capacity of lead were 98% and 68.07 mg/g, respectively. Adsorption data obtained were analyzed with Langmuir and Freundlich isotherm equations. The equilibrium data are fitted by Langmuir isotherm in a superior way than that of Freundlich isotherm. The results show that homogeneous adsorption of the metal ion favors heterogeneous adsorption. The maximum adsorption capacity of iron oxide NPs was calculated through Langmuir isotherm was Q_{max} (68.07) mg/g. Moreover, the adsorption of metal ions with time was also analyzed with the pseudo 1st and pseudo 2nd kinetic equations. The kinetic data are fitted more in the pseudo 2nd order reaction. Adsorption capacity calculated through pseudo 2nd order equation was qe (51.81) mg/g. This literature verifies that NPs synthesized from scrap iron as precursors prove to be an attractive option for removing heavy metals.

Keywords: nanoparticles, green synthesis of nanoparticles, kinetic study, isotherm study, scrap iron precursors, heavy metals removal.

Introduction

As human population increases, the rapid growth of industries and agricultural activities contribute to serious pollution in the environment that is mainly in the water bodies, as an enormous volume of wastewater polluted with several heavy toxic metals are let off daily into the environment through various industrial operations. Considering the elimination of these contaminated heavy metals continuous studies and research has been going on for adsorbents that are efficient and eco-friendly. Mercury, cadmium, lead, arsenic, and chromium are considered to be significant to public health-inducing collective damage to the parts of the body, even at an inconsiderable

*Corresponding author. E-mail: *dassneha30@gmail.com*

magnitude of revelation (Zeng et al., 2021). Natural water is polluted via means of toxic heavy metals through human activities and various industrial applications (Neyaz et al., 2014). Lead (II) is one of the non-essential and most toxic heavy metals which can cause health problem, exposure is detrimental to several organs of the human body viz, gastrointestinal tract, nervous system, liver, kidney, reproductive system and brain (Anayurt et al., 2009; Jumina et al., 2020). It can also cause some other acute and chronic disorders like anemia, encephalopathy, hepatitis, nephritic syndrome, sterility, abortion, stillbirths, and neonatal deaths (He et al., 2020; Ihsanullah et al., 2016). Most of the water streams that are contaminated by lead Pb (II) come from the discharge of industrial wastewater related to mining, electroplating, metal processing, painting, textile production, batteries manufacturing, pesticides, and fertilizers (Sarkar & Sarkar, 2013). Numerous treatment approaches have been enforced to treat the water and wastewater incorporating heavy metals, including chemical precipitation, exchange of ions, chemical oxidation, reverse osmosis, ultrafiltration, electrodialysis (Gunatilake, 2015; Kumar & Mondal, 2020; Mahurpawar, 2015). Among all these, adsorption is one of the most efficient methods. The quality and effectiveness of the adsorbents decide the efficiency and performance of the adsorbents in removing heavy metals. The maximum type of adsorbents is ineffective either due to their diffusion limitation or insufficient active sites available. Due to the difficulty in separation of adsorbent from water makes the adsorbents expensive (Kataria & Garg, 2018). A next generation of nanoadsorbent has been created with recent advance in nanotechnology. Several adsorbents including xanthate-modified magnetic chitosan (Zhu et al., 2012), Fe_3O_4 nanoparticles loaded saw dust carbon (Kataria & Garg, 2018), tea extracts are being used for green synthesis of iron nanoparticles (Huang et al., 2014), functionalized carboxylate ferroxane nanoparticles (Moattari et al., 2015), macrofungus (Lactarius scrobiculatus) biomass (Anayurt et al., 2009). Magnetic activated carbon loaded with tungsten oxide nanoparticles (Saleh et al., 2017), polyamide graphene composite as a novel adsorbent (Saleh et al., 2017) are few examples. Nanoadsorbents having characteristics like surface modification, environment friendly, low-cost production, and the magnetic property have gained a lot of interest. Small size magnetic nanoparticles have a larger surface area, high magnetic property, easy synthesis, low toxicity, reusable efficiency, low cost, and easy to separate from aqueous medium. Magnetic nanoadsorbent have been developed from various methods, but these conventional approaches have many drawbacks such as high cost of production, large energy requirement, low production, use of toxic chemicals, and creation of hazardous by-products (Huang et al., 2014; Martínez-Cabanas et al., 2016). Therefore, there is a need for an economical, ecological and viable way for the synthesis of the nanoadsorbent. Recently green synthesizing, i.e., plant extracts and biowastes of the nanoparticles has been showing a very promising solution for the synthesis of magnetic nanoparticles such as rice casing, pine fragment, pomegranate peel, sawdust, etc. (Fahmy et al., 2018). The metal ions get reduced more readily by the reducing and stabilizing agents in the extracts of plants. The strong antioxidants such as polyphenols, amino acids, nitrogenous bases obtained from various plants, herbs, and spices act as reducing and capping agents for the nanoparticles (Herlekar et al., 2014). Two main challenges that has to be overcome while synthesizing super magnetic iron oxide nanoparticle. One is defined as an experimental condition that should be there so that size can be controlled, and the second is to select that process so that synthesis can be done at an industrial level. Synthesis of nanoparticles are governed by many processes that are co-precipitation, reactions in a constrained environment, polyol methods, flow injection synthesis, aerosol/vapor methods (Wu et al., 2008). Co-precipitation is recognized as more feasible method as it comprises of mixing ferric and ferrous ions in 1:2 molar ratios in extreme basic solutions at room temperature or at elevated temperature (Hasany et al., 2013).

In this study, a low-cost green synthesis method was achieved for the synthesis of magnetite nanoparticles by using scrap iron as a precursor with a high yield and production rate of nanoadsorbent. Scrap iron is a waste material, and the first time it is used for the green synthesis of NPs successfully. Magnetite nanoparticles were synthesized by implementing the co-precipitation method, and pomegranate peel extracts were used as a reducing and capping agent of the same. The potentiality of the nanoparticles to separate lead from the aqueous medium was observed, and the regeneration and reusability of the synthesized nanoparticles were also explored.

1. Methodology and materials

1.1. Materials

Pomegranate peel used in this study was collected from the local market Durgapur city. The scrap iron that was used for the synthesis of iron oxide NPs was collected from the workshop of NIT Durgapur (India). Chemicals of analytical grade and deionized water were used in the study.

1.2. Preparation of iron solution from scrap iron

For the synthesis of magnetite nanoparticle, a mixture of $FeCl_3$ and $FeCl_2$ with a volume ratio of 1.7:1 was used as a precursor. Initially, 1 M of $FeCl_2$ was prepared by dissolving 6 gm of scrap iron in 2 M 100 ml HCl and $FeCl_3$ were obtained by adding 1.68 gm of $KMnO_4$ in 50 ml of already prepared $FeCl_2$ solution.

1.3. Preparation of pomegranate peel extracts

Deionized water was used to eliminate the dust particles from the collected pomegranate peel pulp and was dehydrated for 15 days at room temperature under dust-free

surroundings. The dehydrated peel was then crushed by using a pestle and mortar and sieved by using a 400-micron sieve. From the obtained dry peel 20 gm of peel, the powder is introduced in 500 ml of distilled water, and it is kept for three hours and then sonicated by using a probe sonicator for ten minutes. The obtained mixture was then filtered by using Whatman filter paper no 41 and centrifuged at 5000 rpm for 20 minutes to eliminate the suspended pomegranate particles and kept in the fridge at 4 ^{o}C for usage in the further process to synthesize iron oxide nanoparticle (Whatman filter paper no 42).

1.4. Synthesis of iron oxide nanoparticles with coating of pomegranate peel extract

The co-precipitation method was used to modify the synthesis of magnetic nanoparticles (Hariani et al., 2013). Pomegranate peel extract was used, which acts as an antioxidizing and reducing agent that inhibits the oxidation of Fe^{2+} by the air in the co-precipitation method, thus eliminating the use of inert atmosphere, which is typically required to prevent the oxidation of ferrous ions. Synthesis was done in the open atmosphere to compensate for the oxidation of Fe^{2+} to Fe^{3+} with a mixture of $FeCl_3$ (63 ml) and $FeCl_2$ (38 ml) volume ratio of (1.7:1). The obtained iron mixture solution was mixed with pomegranate peel extracts (100 ml) in a volumetric ratio of 1:1, and the solution was then heated at a temperature of 80 ^{o}C using a hot air oven (Labard Instruchem Pvt. Ltd). The pH was adjusted to 12 by adding 1.0 M of NaOH drop-wise to the solution. The solution mixture was then stirred using a magnetic stirrer continuously for 30 minutes to homogenize it and complete the reaction process. After this, the gained precipitate was composed via magnet and washed numerous times by using distilled water and ethanol to remove the impurities and kept drying in an incubator for two days at a temperature of 50 °C. The obtained NPs were then crushed using pastel and mortar and sieved using a 75 μm sieve and stored in closed containers for further use. Uncoated nanoparticles were also synthesized under similar conditions for the comparative study.

1.5. Characterization of obtained nanoparticles

The phase purity and crystalline nature of synthesized nanoadsorbent were done by using an X-ray diffractometer (PANalytical XPert Pro Basic X-ray Powder Diffraction, U.K) with Cuk-kalpha radiation source were used in the 2θ range between 20° to 70°, with a scan speed of 2°/min, and scan step of 0.025°. Dynamic light scattering technique (DLS) was used. The particle size distribution of the synthesized nanoparticles and the particle size distribution curve was obtained by using (Zetasizer, Malvern U.K). The morphology and the size of nanoparticles were analyzed by FESEM using (Sigma Carl Zeiss, U.K.). UV-vis spectra Shimadzu (2450 SHIMADZU Corporation, Japan) spectrometer recorded the synthesized iron nanoparticles. BET surface area, pore volumes, and pore size distribution of the synthesized nanoparticles were determined by using a computer-controlled automated porosimeter (NOVA 1000e Quantachrome Instrument, USA).

1.6. Batch adsorption experiments

A Pb (II) stock solution of 1000 mg/l was prepared by dissolving 1.614 g of lead nitrate $Pb(NO_3)_2$ in 1 liter of distilled water. Batch adsorption was used to analyze the effect of various operating conditions on the adsorption process. Various adsorption experiments were carried out in this study to examine the outcome of the experimental condition on achieving the maximum amount of Pb (II) removal. For an effective method of removing Pb (II), different parameters such as the effects of pH, the dosage of adsorbent, initial concentration of Pb (II), contact time, and temperature have been considered. In this experiment, 0.05 gm of magnetic nanoadsorbent was added in 50 ml of the Pb (II) solution with a concentration of 50 mg/l in 250 ml of a flask, and the pH was adjusted to 6 by means of 1 M of NaOH and 1 M of HCl. Then it was kept in a BOD shaker at an agitation rate of 120 rpm for 1 hour 30 minutes. After that, clear supernatant solutions were collected by using a permanent magnet and analyzed for metal concentration using AAS for respective dosage, and equilibrium concentration was measured. The removal percentages were calculated by using Equation (1).

$$\text{Removal efficiency } R\% = \frac{C_o - C_e}{C_o} \times 100\,, \tag{1}$$

where C_o is the initial concentration of Pb (II) ions in (mg/l), C_e is the residual concentration of Pb (II) ions in solution after equilibrium (mg/l). The metal adsorption capacity q_e = mg/g of each combination for adsorption of Pb (II) ions at equilibrium was determined using Equation (2) (Guler, 2017).

$$q_e = \frac{C_o - C_e}{m} \times V, \tag{2}$$

where V indicates the volume of solution (L), and m represents the mass of the adsorbent in (g).

2. Results and discussions

2.1. Characterizations of nanoparticles

2.1.1. XRD analysis

The coated and uncoated nanoadsorbent underwent XRD analysis to know the crystalline structure and phase purity of the coated and uncoated nanoparticles. The XRD pattern of the pomegranate peel (PoP's) coated nanoparticles is shown in Figure 1a. The X-ray diffraction pattern of PoP's coated nanoparticles displays six relative peaks in the 2θ region of 20–70°. The prominent peak of the powdered nanoparticle was at the 2θ value of 35.60 is the attribute to the crystalline plane with Miller indices value of 311. The other peaks are observed 30.23°(202),

43.24°(400), 53.59°(422), 57.10°(333), 63.79 reflection planes of PoP's coat, which is matched well with the typical diffraction data of cubic inverse spinel Fe_3O_4. The peak (2θ) of the nanoparticle which is located at 2θ°= 22°, and 25° may relate to the amorphous organic compounds adsorbed from the pomegranate peel extracts as a capping agent/stabilizing agent by the iron oxide nanoparticles similar pattern was found when green tea waste used as a capping agent (Fan et al., 2017). While the uncoated nanoparticle shows the formation of goethite may be due to oxidation of ferrous ion in the open atmosphere, as shown in Figure 1b. The obtained magnetite Fe_3O_4 is a combination of FeO and Fe_2O_3. The uncoated iron oxide nanoparticle may undergo oxidation as the synthesis has been performed in the open atmosphere. FeO can be oxidized to Fe_2O_3 or $Fe(OH)_2$ according to the reaction given below (Sulistyaningsih et al., 2017).

$$2(FeO \cdot Fe_2O_2 + \frac{1}{2}O_2 \rightarrow 3Fe_2O_3; \quad (3)$$

$$Fe_3O_4 + \frac{1}{4}O_2 + 4\frac{1}{2}H_2O \rightarrow 3Fe(OH)_3. \quad (4)$$

2.1.2. Particle size distribution

The particle size distribution and the average size of the PoP's coated and uncoated nanoparticles were compared using the particle size distribution curve obtained by the DLS method. Figure 2a clearly shows that the calculated mean size of the PoP's coated NPs is 36.5 nm while the uncoated NP's in Figure 2b mean size is 66.6 nm. The size

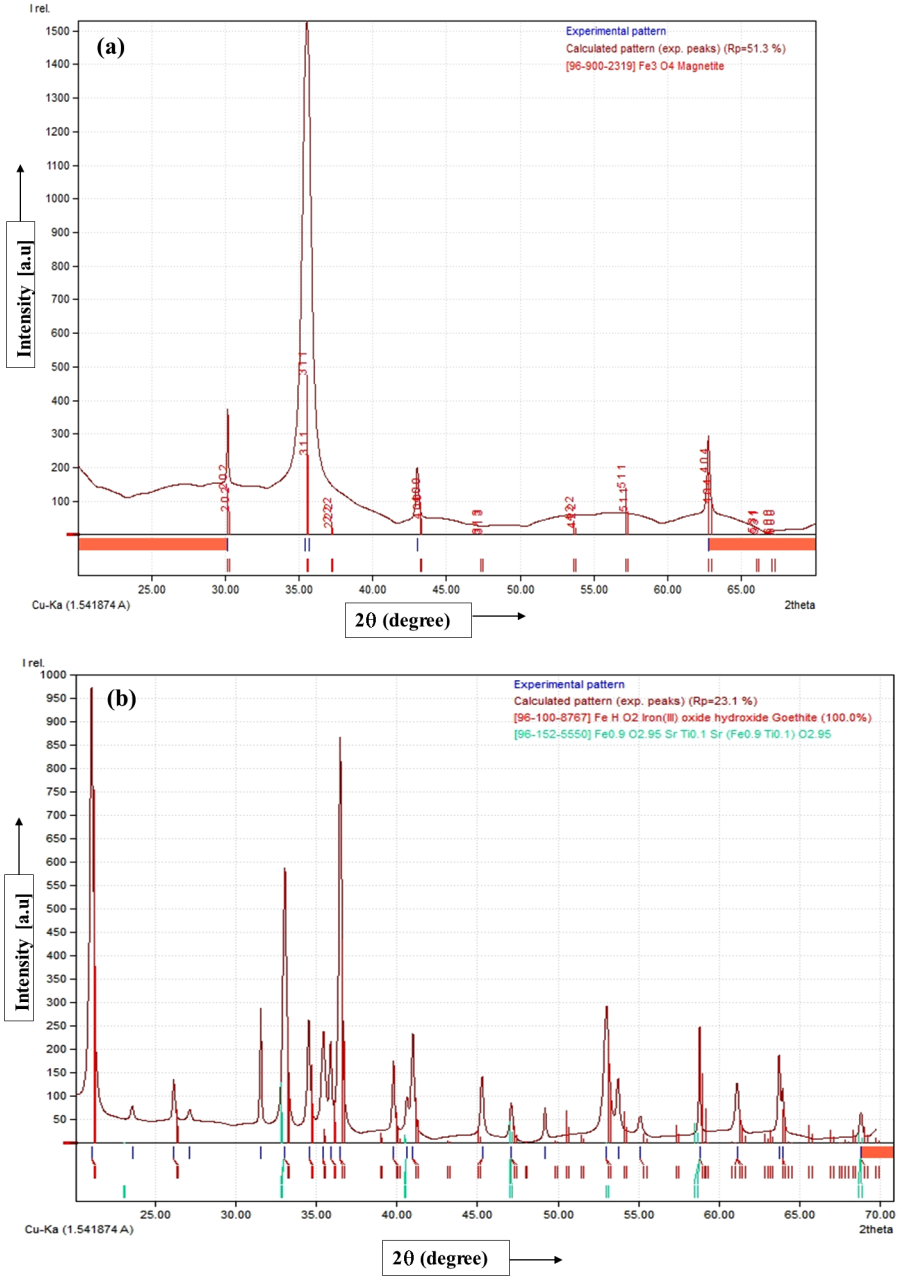

Figure 1. XRD pattern of (a) coated (Fe_3O_4) nanoparticles, (b) uncoated (Fe_3O_4) nanoparticle

distribution obtained by DLS for the particles synthesized without using PoP's extract may be due to particle agglomeration of the iron oxide nanoparticles.

2.1.3. FE-SEM analysis

The morphology and the size of the synthesized iron oxide nanoparticle were a confirmation to be almost spherical shaped in nature and uniform in size and as in Figure 3.

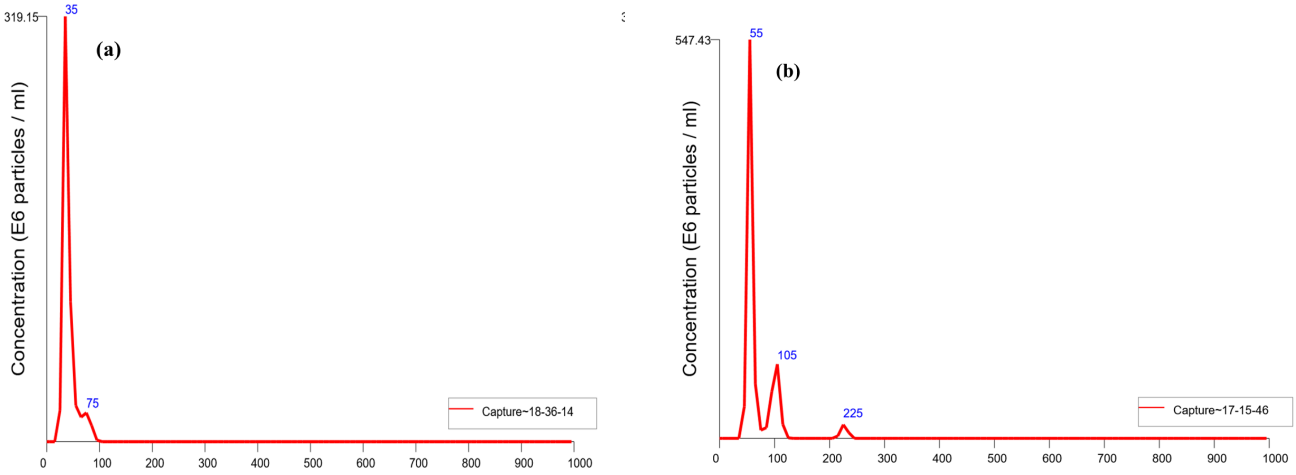

Figure 2. Particle size distributions curve of synthesized nanoparticles determined by DLS analysis (a) coated NPs, (b) uncoated NPs

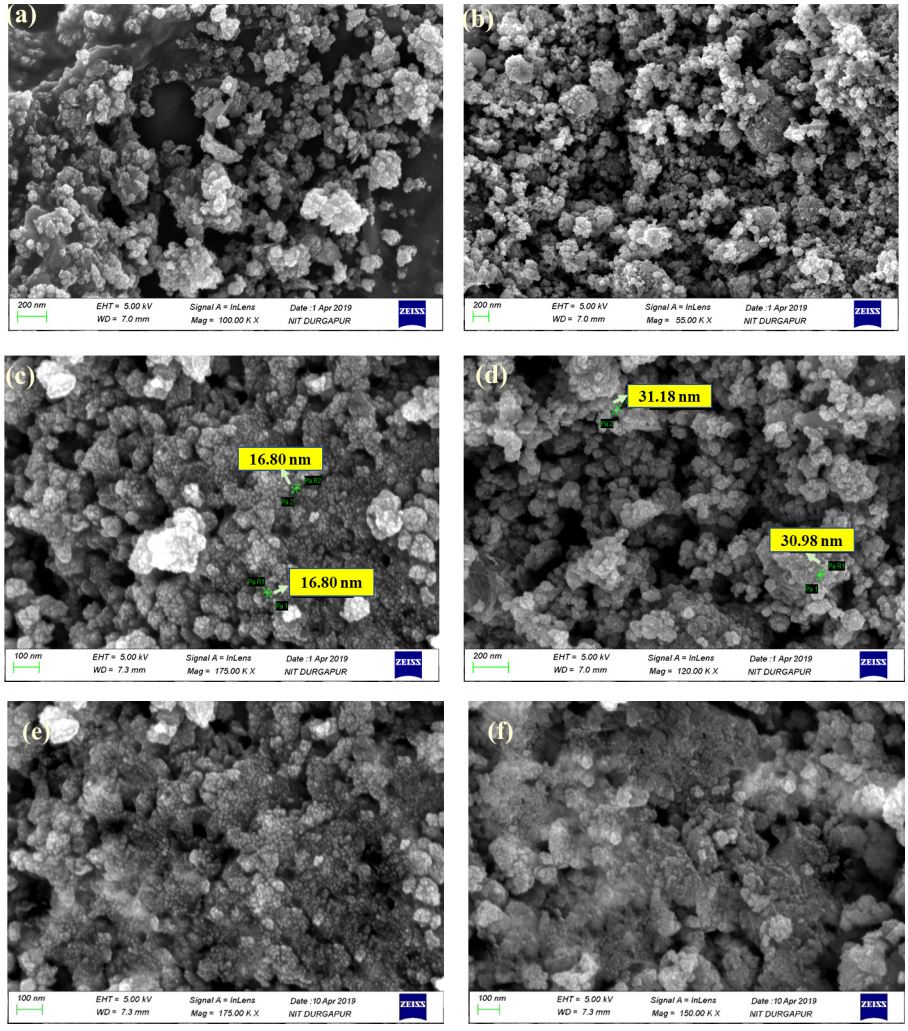

Figure 3. FE-SEM image of iron oxide (Fe_3O_4) NP's at different magnification scale (a), (b), (c) and (d) before adsorption, (e) and (f) after adsorption

Presence of microspores and mesopores in Figure 3 indicates that the pore diffusion is a rate-limiting step. Non-uniform distribution of nanoparticles indicates the enhancement of the surface area, which again increases the uptake capacity of the adsorbent. It can be seen that the particle size distribution curve of Fe_3O_4 NP's indicates that the diameter of synthesized Fe_3O_4 NP's ranges from 15 to 31 nm. The SEM image of post adsorption (Figure 3: (e) and (f)) indicated that the pores of the adsorbent were saturated due to the adsorption process.

2.1.4. BET analysis

The specific surface area of the particles is the summation of the areas of the exposed surfaces of the particles per unit mass. There is an inverse relationship between particle size and surface area. Nitrogen adsorption is used to measure the specific surface area of a powder. The method of Brunauer–Emmett–Teller (BET) is commonly used to determine the total surface area the specific surface area of iron oxide nanopowder calculated by using the multipoint BET equation. The specific surface area obtained is 46.856 m^2/g. Based on the BJH academic model, the property of the cumulative pore specific surface area, cumulative pore volume, average pore diameter, and the probability pore size of pores were calculated summarized in Table 1. It was found that the average pore volume was 0.2113 cm^3/gm and the average pore width was 9.019 nm, which represents that the synthesis material has a good pours structure with more surface area for adsorption (Prathna et al., 2017).

Table 1. BET measurement results

Surface area	BET surface area (m^2/g)	46.856
	BJH adsorption cumulative surface area of pores (m^2/g)	33.63
	BJH desorption cumulative surface area of pores (m^2/g)	41.73
Pore volume	Single point adsorption total pore volume of pores (cm^3/g)	0.2113
	BJH adsorption cumulative volume of pores (cm^3/g)	0.203
	BJH desorption cumulative volume of pores (cm^3/g)	0.210
Pore size	Adsorption average pore width (nm)	9.019
	BJH adsorption average pore radius (nm)	1.599
	BJH desorption average pore diameter radius (nm)	7.291

The N_2 absorption-desorption isotherms of iron-oxide nanoparticles were measured by using the static volumetric adsorption analyzer. Figure 4 shows the typical nitrogen sorption isotherms of iron-oxide nanoparticles. It shows that the sample shows distinctive IV adsorption in the low-pressure region ($P/P_0 < 0.8$). The graph shows that the isotherms are comparatively flat where the adsorption and desorption isotherms completely superposition, which indicates that the adsorption of the samples mostly occurs in the micropores. At the relative high-pressure region ($P/P_0 > 0.8$), due to the capillary agglomeration phenomenon, the isotherms increase rapidly and form a lag loop which can be seen in Figure 4.

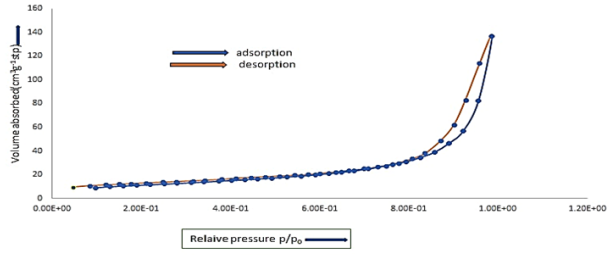

Figure 4. N_2 gas adsorption-desorption isotherm for magnetic ironoxide nanoparticle

The point of zero charges (ZPC) of Fe_3O_4 nanoparticles, obtained from Figure 8a of initial (pH-final pH) vs. initial pH and the value of (pHzpc) was found to be pH (5.7). Moreover, the adsorption of Pb (II) in highly basic solution is more than in acidic solution because the surface of the adsorbent becomes negative at pH < pHzpc, and also in the basic solution, the deportation of –OH group happens at the surface of the nanoparticle employing rise in pH of the solution.

2.1.5. Analysis of synthesized Fe_3O_4 by UV-vis spectrophotometer

As in the green synthesis of iron oxide nanoparticles, plant biomolecules are involved in synthesizing and stabilizing nanoparticles (Yew et al., 2020). In this study, Fe_3O_4 NPs were green synthesized using the pomegranate peel extracts with precursor molecules $FeCl_2$ and $FeCl_3$. The bioreduction of Ferric ions in aqueous solution was measured using Visible Spectroscopy in the range of 190–700 nm. The peak was obtained at 258 nm, which confirms the formation of iron oxide nanoparticles. Figure 5 similar peak has been observed by (Das & Rebecca, 2018).

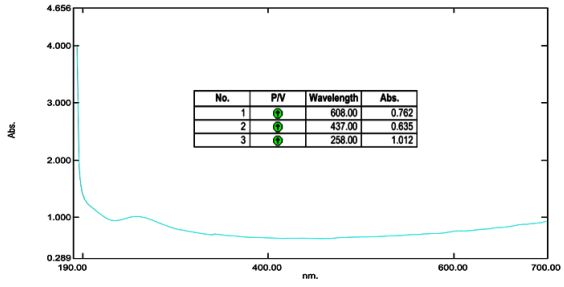

Figure 5. The UV-vis spectra of synthesized Fe_3O_4 NPs

2.2. Adsorption mechanism

A possible mechanism for forming the magnetite NPs by using PoP's extract and scrap iron is represented in Figure 6. Figuer 6 showing the synthesis of magnetite $FeCl_3$

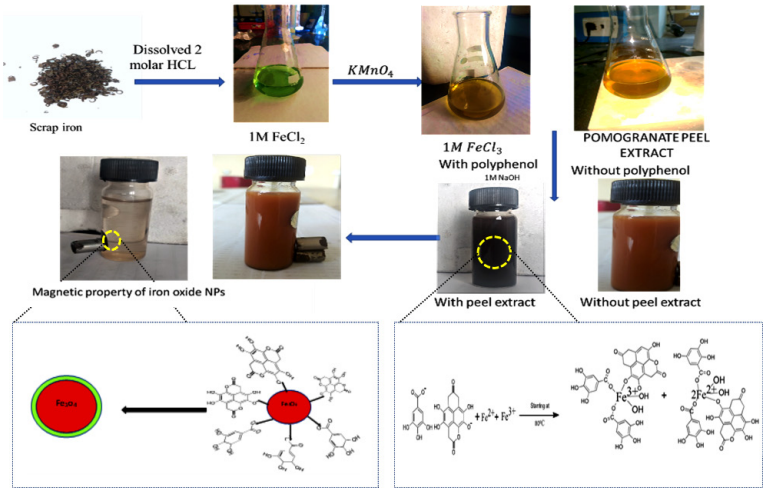

Figure 6. Representation of the formation mechanism of magnetite NPs by means of PoP's peel extract and scrap iron precursors along with the synthesis of magnetite iron oxide NPs by using scrap iron in PoP's extract

and $FeCl_2$ using PoP's extracts. Approximately 48 phenolic compounds (anthocyanins, gallotannins, hydroxycinnamic acids, hydroxybenzoic acids, hydrolysable tannins i.e. ellagitannins, and gallagyl esters) have been recognized in pomegranate covering and further anatomical portions of the fruit (Akhtar et al., 2015). The peel of the pomegranate compromises about 50% of fruit weight, characterized by the existing high molecular weight phenolics, complex polysaccharides, flavonoids, and considerable quantities of microelements that on the entire reveal strong anti-mutagenic, antioxidant, antimicrobial features. The compounds like Ellagic acid and Gallic acid are the major photochemical existing in aqueous pomegranate peel extract. The synthesis of Fe_3O_4 was carried out at a temperature of 80 °C. At this temperature, the carbon C of polyphenol and OH of NaOH would be included in the reaction process and, hence, strife in forming bonds between COO…Fe^{3+} and COO– R…Fe^{2+} forming bond between OH^-…Fe^{3+} and OH^-…Fe^{2+}, which results in the development of ferrous hydroxide [$FeOH_2$] and ferric hydroxide [$Fe(OH)_3$].

Lastly, due to dehydration (–H_2O) magnetite NPs were formed from ferric hydroxide and ferrous hydroxide in the reaction mixture as by the given equation.

$$2Fe^{3+} + Fe^{2+} + 8OH^- \rightarrow$$
$$2Fe(OH)_3 Fe(OH)_2 \rightarrow Fe_3O_4(S) + 4H_2O. \quad (5)$$

2.3. Lead removal process

2.3.1. Effect of initial concentration on the removal of Pb (II)

The removal efficiency was high (>97.7%) through the initial concentration of 50 mg/l, but the efficiency declines from 97.7% at 50 mg/l to 91% at 70 mg/l in IONP-C (iron oxide NPs coated). In Figure 7a, $FeHO_2$ efficiency was 80%. This is because the available surface of the adsorbent is satisfactory to adsorb maximum Pb (II) ions at low initial concentration, which results in filling the available sites IONP-U (iron oxide NPs uncoated). Therefore, the adsorption is more up to a definite extent. Suppose there is further addition in the initial concentration of the available sites, in that case, it becomes scarce to adsorb additional metal ions, resulting in suspension of these ions, and no more metal ions possibly will be adsorbed. Various studies revealed that Pb (II) ions removal efficiency depends on initial concentration, and with an increase in initial concentration, there is a decreasing trend in adsorption (Ahmad & Mirza, 2018).

2.3.2. Effect of contact time

The period for the adsorption of lead ions was conducted on Fe_3O_4 nanoparticles in an aqueous solution. It can be distinguished that when the equilibrium reached 45 min, the removal of the Pb (II) ions was improved with the rise of the contact time from Figure 7b. More than 55% of the lead gets absorbed in the first 3 min of contact time, and after 35 min of contact, the removal percentage was more than 90%. The removal was seen 98% when the equilibrium time reached 45 min. After that, adsorption remains the same with a slight decrease at 90 min. Similar results were obtained by (Nassar, 2010) as the equilibrium was achieved very quickly as a result of the compact size of the nanoparticles (Nassar, 2010). This condition is favorable for the diffusion of metal ions from the solution into the active sites of the adsorbent, and the adsorption is dominated by external adsorption as no pore's dissemination was monitored to slow down the adsorption.

2.3.3. Adsorbent dosage effects

The adsorbent quantity stands as one of the significant operational parameters as it governs the adsorption capacity of the adsorbent meant for a given initial concentration of adsorbate. The result of adsorbent dose on Pb (II) adsorption is demonstrated in Figure 7c. The result shows that

as the dose was increased from 0.02 g to 0.05 g (IONP-C (iron oxide NPs coated)), the adsorption efficiency increased up to 98.434%. This shows that an increase in adsorption is majorly achieved due to an increase in surface area and the available adsorption site of the adsorbent. The removal efficiency of $FeHO_2$ remained 78.92% which was lesser than the adsorption capacity of the coated nano adsorbent IONP-U (iron oxide NPs uncoated).

2.3.4. Effect of pH

Different pH was maintained to study the adsorption of Pb (II) ions, as the pH of the solution plays a vital role in the adsorption of various metal ions. Surface chemistry and metal ions solution chemistry changes significantly with a change in pH. The pH value ranging from 2 to 6 for Pb (II) solution was adjusted. Figure 7d shows that the removal percentage of Pb (II) by Fe_3O_4 follows a sharp increase from 4% to 97.8% at pH 2 to 6, respectively. The occurrence of the metal hydrolysis precipitation leads to lead removal. pH > 6 introduces uncertainty concerning adsorption versus precipitation of lead (Rajput et al., 2016). The electrostatic attraction between the charged adsorbent surface presides over the process of Pb (II) ions on the Fe_3O_4 nanoparticles.

2.3.5. Effect of Co-existing cation

As groundwater comprises more than one cation and the occurrence of other cation might interfere with the removal efficiency of the Pb (II) metal ions, to check this, following co-existing metal ions on Pb^{2+} adsorption was studied. Co-existing cations Ni^{+}, Mn^{2+}, and Cr^{3+} were no considerable effect on the removal of Pb shown in Figure 8b. Heavy metals Cr > Mn > Ni were removed up to 93%, 31.3%, 22.15% respectively. The adsorption variability varies with the metal ions, and it depends on several factors: molecular mass, charge, and hydrated ionic radius (Shi et al., 2018).

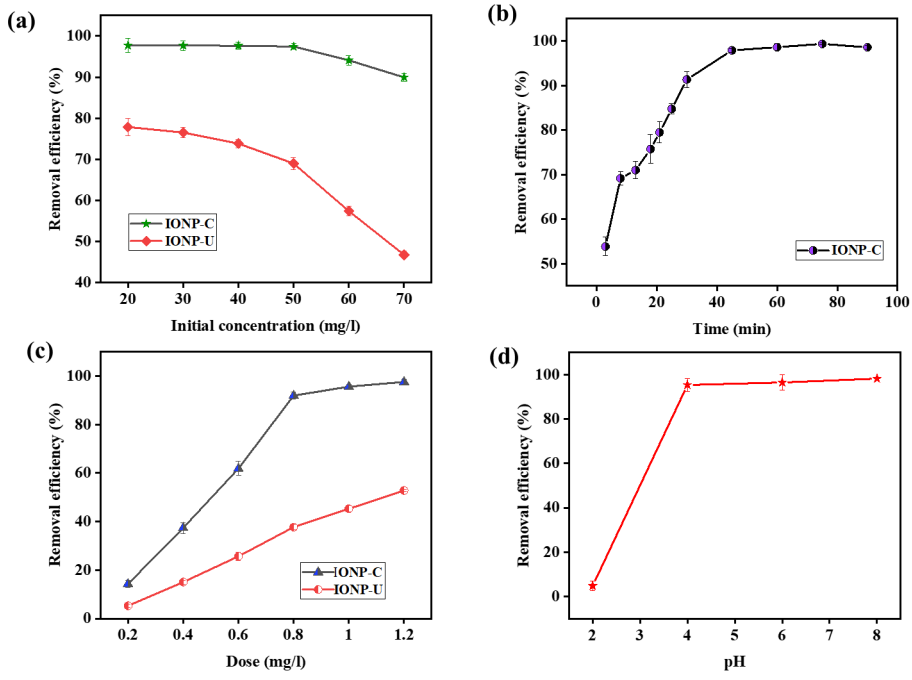

Figure 7. (a) Effect of adsorbent dose, (b) Effect of initial concentration, (c) Effect of pH, (d) Effect of contact time

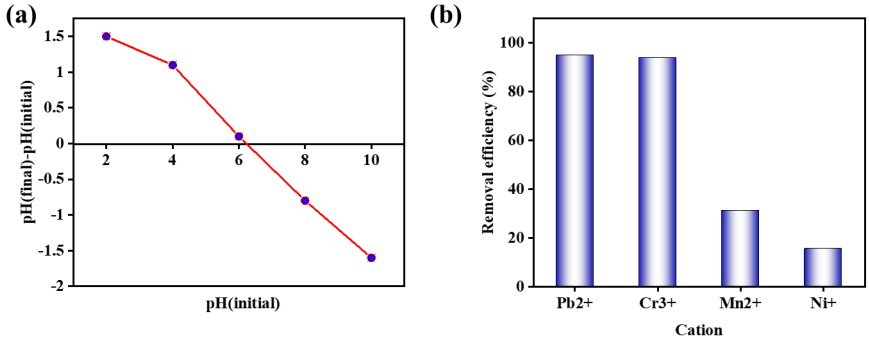

Figure 8. (a) pH_{zpc} zero-point charge of magnetic oxide NPs, (b) Effect of the presence of other metal ions on the removal of lead (II) by Fe_3O_4

2.4. Kinetics and Adsorption Isotherm Studies

2.4.1. Kinetic adsorption

To determine the rate constant and evaluate the diffusion process, a kinetic study was performed by pseudo 1st. The pseudo 2nd order was applied to experimental data via fluctuating the contact time among the adsorbate (Pb) and adsorbent. Pseudo 1st order and pseudo 2nd order (Fierro et al., 2008; Mondal & Mahanta, 2017) in the linear form expressed as

$$\log\left(q_e - q_t\right) = \log q_e - \frac{k_{ad}}{2.303}; \tag{6}$$

$$\frac{t}{q_t} = \frac{1}{h} + \frac{1}{q_e}t, \tag{7}$$

where q_e and q_t (mg/g) are the adsorption of Pb at the equilibrium time and contact time respectively, k_{ad} (min^{-1}) is the pseudo 1st order rate constant and h ($g{\cdot}mg^{-1}min^{-1}$) is the 2nd pseudo rate constant.

Value of k_{ad} and q_e in pseudo 1st order was calculated from the pseudo first-order kinetic Equation (6), and R^2 was determined from the slope of log (q_e–q_t) vs t as shown in Figure 9a. The kinetic model calculated the values of h and q_e by using Equation (7). In Figure 9b, the slope of the pseudo 2nd order reaction shows good linearity with the co-relation coefficient value R^2. This indicates that the removal of Pb follows the pseudo 2nd order kinetics and the maximum removal efficiency obtained q_{max} = 51.81 mg/g. The kinetic model and parameters are mentioned in Table 2. The whole adsorption process supports the assumption chemisorption process by the exchange of ions.

2.4.2. Adsorption isotherm

In order to analyse the experimental sorption equilibrium data and to attain some substantial evidence of the surface properties and its affinity for the examined metal ions, Langmuir and Freundlich isotherm models were applied. For determining the adsorption isotherms of Pb (II), different initial concentration of adsorbate ranging from 20 to 70 mg/l and adsorbent 0.05 g at 100 rpm at 298K for 90 min was studied. The uptake capacity qe of the adsorbent was calculated by using Equation (8) (Kamilya et al., 2021).

$$\frac{1}{q_e} = \frac{1}{q_{\max}} + \frac{1}{C_e b q_{\max}}, \tag{8}$$

where q_e is the amount of adsorbed (mg/g), C_e is the equilibrium concentration of the adsorbate in the solution (mg/l) constant, q_{max} is the maximum adsorption capacity in (mg/g) under the experimental condition, b is the constant related to the affinity of the binding sites (L/mg). A straight line is obtained when $1/q_e$ was plotted against $1/C_e$. Figure 11a shows the adsorption of Pb (II) followed the Langmuir isotherm. q_{max} and b were calculated from the slope and intercept of the linear plots by using Equation (8). Langmuir parameters determine the affinity between the adsorbate and adsorbent by using dimensionless separation factor (R_L).

$$R_L = \frac{1}{bC_o}, \tag{9}$$

where C_o is the initial concentration of metal ion and b is Langmuir constant value, implies the nature of the isotherm four possibilities for the R_L value (1) unfavourable adsorption ($R_L > 1$), (2) favourable adsorption ($0 < R_L < 1$), (3) linear adsorption ($R_L = 1$), (4) irreversible ($R_L = 0$).

The linear form of Freundlich isotherm was calculated by following Equation (10) for the experimental data.

$$\log q_e = \log K_F + \frac{1}{n}\log C_e, \tag{10}$$

where K_F and n are the constants of Freundlich adsorption isotherm, which signifies heterogeneous adsorption capacity (mg/g) and adsorption intensity (L/mg). The plot of the log of qe against log C_e is employed to find the value of K_F and the value of n from the intercept and slope the value of n, K_F, and R^2 (regression coefficient) were calculated in Figure 10b. It can be perceived from Figure 10a that the experimental data fit the Langmuir adsorption isotherm well. The maximum adsorption capacity of Pb (II) was found to be 68.07 mg/g. The value of R^2 = 0.97 suggests the homogenous adsorption of Pb (II) on the surface of magnetic nanoparticles. R_L value obtained (0.0034) shows that R_L (mentioned in Table 3) is less than 1 for adsorption of Pb (II) onto Fe_3O_4 nanoparticles; therefore, the process is favorable.

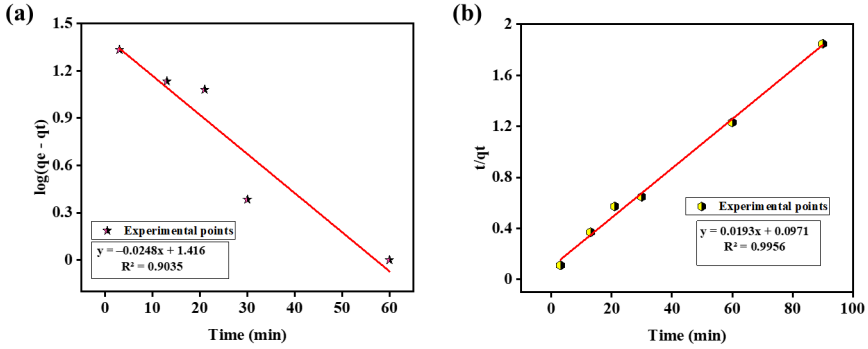

Figure 9. The plots showing Kinetic adsorption of lead (II) by Fe_3O_4 (a) Pseudo first order, (b) Pseudo second order

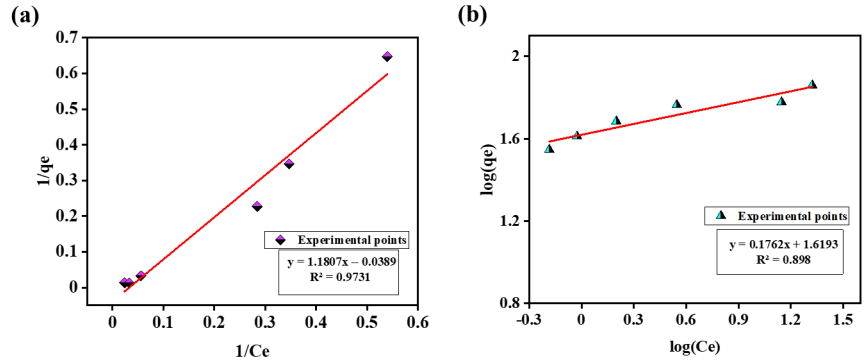

Figure 10. Plot showing (a) Langmuir and (b) Freundlich isotherm values for lead (II)

Table 2. Kinetic model and parameter values for the lead (II) adsorption on the magnetic NPs

Kinetic models	Parameters	Fe_3O_4 NPs
Pseudo 1st order	q_e (cal)	26.06
	k_{ad} (min^{-1})	0.057
	R^2	0.9035
	Adjusted R^2	0.8713
Pseudo 2nd order	q_e (cal)	52.81
	K ($g{\cdot}mg^{-1}min^{-1}$)	0.043
	R^2	0.9956
	Adjusted R^2	0.9944

Table 3. Langmuir and Freundlich isotherm values for lead (II) adsorption on magnetic NPs

Isotherm	Parameters	Fe_3O_4 NPs
Langmuir isotherm	Q_{max} (mg/g)	68.07
	b (L/mg)	1.63
	R_L	0.0034
	R^2	0.975
	Adjusted R^2	0.966
Freundlich isotherm	K_F (mg/g)	41.6
	n (L/mg)	5.67
	R^2	0.898
	Adjusted R^2	0.8724

2.5. Adsorption mechanism of lead (II) ions

The Pb (II) ions endure association and hydrolysis in aqueous solution, as per the subsequent reactions

$$Pb^{2+}(S) + nH_2O \leftrightarrow Pb(H_2O)_n{}^{2+}(s); \quad (11)$$

$$Pb(H_2O)^{2+}{}_n(s) \leftrightarrow Pb(H_2O)^{n-1} + H^+; \quad (12)$$

$$b^{2+} + mH_2O \leftrightarrow Pb(OH)^{2n-1}{}_m + mH^+. \quad (13)$$

In many studies, it's been observed that at pH > 6.5 Pb gets precipitated in $Pb(OH)_2$ and at pH < 6.5 Pb^{2+} and $Pb(OH)^+$ are present in the aqueous solution (Nassar, 2010). Also, the surface of the Fe_3O_4 nanoparticle can go protonation and deprotonation as per the reaction.

$$H_2O + M-O^- \underset{OH^-}{\overset{H^+}{\leftrightarrow}} M-OH \underset{OH^-}{\overset{H^+}{\leftrightarrow}} M-OH^{2+}, \quad (14)$$

where H^+ and OH^- are the acidic and basic determining factors of the solution.

The electrostatic attraction caused is the primary reason behind adsorption. When the solution is highly basic, a strong electrostatic attraction occurs amongst the negatively surface of magnetite nanoparticle and positive lead (Pb^{2+}) ions. The proposed mechanism is presented in Figure 11. As the solution becomes more and more acidic, the surface of the adsorbent becomes more and more positive, and the number of negatively charge site decreases. The adsorption is not favorable for Pb (II) ions as the surface of the nano adsorbent is positively charged. And also, at higher pH, H^+ ions strive with the Pb (II) ion for the adsorption site, which results in lowering of the adsorption. A comprehensive study of removal efficiency and maximum adsorption have been mentioned in Table 4 (present study and literature survey).

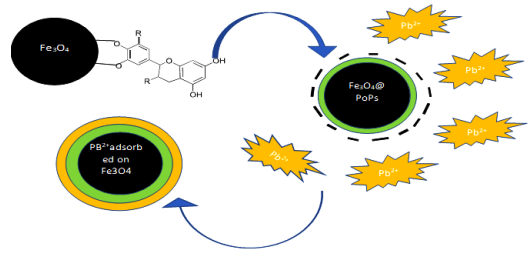

Figure 11. Proposed mechanism of lead (II) removal by using Fe_3O_4 NPs as adsorbent

2.6. Desorption and reusability of nanoadsorbent

At lower pH, i.e., in an acidic medium, the Pb removal is low due to interference of H^+ with Pb ions. The Pb ions could be replaced by H^+ ions present in solution by the

Table 4. Comparative table showing Pb removal using different adsorbents

Sl. No.	Adsorbent	q_m (mg/g)	Removal Efficiency	Reference
1.	Fe_3O_4 – (POP_S) coated NP_s	51.81	97.7%	Present Study
2.	Fe_3O_4@chitosan nanocomposites	31.6	94.6%	Liu et al. (2009)
3.	L-Cysteine Functionalized (Fe_3O_4) NP_s	18.8	97%	Bagbi et al. (2017)
4.	Magnesium Oxide Nanoparticles	21.78	94.78 %	Dargahi et al. (2016)
5.	Novel-modified magnetic	14.03	76.72 %	Jafarinejad et al. (2017)
6.	Homogenous in-situ generated ferrihydrite	64.77	97.8%	He et al. (2020)
7.	Reusable gel cation exchange resin containing nano-scale zero valent iron	22.5	87%	Chanthapon et al. (2018)
8.	Iron Oxide Nanoparticles (α-Fe_2O_3)	21	97.5%	Ali et al. (2021)
9.	Iron oxide nanomaterials with cobalt and nickel doping	19.3	94.5%	Chen et al. (2019)
10.	PAN nanofibers	13.96	97.89%	Moradi et al. (2018)

ion exchange process to know the desorption capacity of nanoadsorbent. 1 M of 50 ml HCL as given by Xu et al. (2012) was added for 45 min, and the desorbed amount of Pb was obtained by using AAS. The amount of Pb recovered was 91%, with no substantial lessening in the adsorption capacity of Fe_3O_4 NPs observed after two cycles of desorption. The reusability of the nanoadsorbent was also observed, and an adsorption efficiency of 90.02% was found after two cycles.

Conclusions

In the present study, magnetite (Fe_3O_4) NPs were synthesized through the green route by co-precipitation method using scrap iron as salt precursors and pomegranate peel extract as the reducing and capping agent. The synthesis of nanoparticles was done at an elevated temperature of 80 °C in an open atmosphere. The obtained nanoadsorbents were employed for the removal of lead from the aqueous medium. Kinetic study revealed that 98% of removal efficiency was obtained at the equilibrium time of 45 minutes. The batch experimental results show that the removal efficiency of Pb (II) from the aqueous solution was pH dependable, initial Pb (II) concentration, contact time, and dose of adsorbent. The sorption is favourable in basic solution as the electrostatic attraction between the charged adsorbent surfaces presides over the process of Pb (II) ions on the Fe_3O_4 nanoparticles. The maximum uptake capacity of 68.07 mg/g was obtained from the Langmuir isotherm model (R^2 = 0.97). Pseudo Second Order Reaction Model is found to be best fit model to delineate the sorption process. 91% of Pb was recovered using 1 M of 50 ml HCL with no substantial lessening in the adsorption capacity of Fe_3O_4 NPs observed after two cycles of desorption. The obtained results corroborate that synthesis of iron oxide nanoparticles process is simple and can be used as promising adsorbent for the removal of lead from wastewater.

Acknowledgements

The authors are obliged to the Director, National Institute of Technology, Durgapur-713209, West Bengal, India, for providing essential support for carrying out the present research.

Funding

This work was supported by grants from the Department of Science & Technology and Biotechnology, Government of West Bengal (Memo No. 231(Sanc.)/ST/P/S&T/5G-19/2017 dated 24/03/2018).

Authors' contributions

Mohd Taqui has performed all the experiments and analyses in the lab. Sandip Mondal and Surbhi Chaudhuri have supervised the research work. Sneha Das and Tuhin Kamilya wrote the paper.

References

Ahmad, R., & Mirza, A. (2018). Facile one pot green synthesis of Chitosan-Iron oxide (CS-Fe_2O_3) nanocomposite: Removal of Pb(II) and Cd(II) from synthetic and industrial wastewater. *Journal of Cleaner Production*, *186*, 342–352. https://doi.org/10.1016/j.jclepro.2018.03.075

Akhtar, S., Ismail, T., Fraternale, D., & Sestili, P. (2015). Pomegranate peel and peel extracts: Chemistry and food features. *Food Chemistry*, *174*, 417–425. https://doi.org/10.1016/j.foodchem.2014.11.035

Ali, A. A., Ahmed, I. S., & Elfiky, E. M. (2021). Auto-combustion synthesis and characterization of iron oxide nanoparticles (α-Fe_2O_3) for removal of lead ions from aqueous solution. *Journal of Inorganic and Organometallic Polymers and Materials*, *31*(1), 384–396. https://doi.org/10.1007/s10904-020-01695-3

Anayurt, R. A., Sari, A., & Tuzen, M. (2009). Equilibrium, thermodynamic and kinetic studies on biosorption of Pb(II) and Cd(II) from aqueous solution by macrofungus (Lactarius scrobiculatus) biomass. *Chemical Engineering Journal*, *151*(1), 255–261. https://doi.org/10.1016/j.cej.2009.03.002

Bagbi, Y., Sarswat, A., Mohan, D., Pandey, A., & Solanki, P. R. (2017). Lead and chromium adsorption from water using L-Cysteine functionalized magnetite (Fe_3O_4) nanoparticles. *Scientific Reports*, *7*(1), 7672. https://doi.org/10.1038/s41598-017-03380-x

Chanthapon, N., Sarkar, S., Kidkhunthod, P., & Padungthon, S. (2018). Lead removal by a reusable gel cation exchange resin containing nano-scale zero valent iron. *Chemical Engineering Journal*, *331*, 545–555. https://doi.org/10.1016/j.cej.2017.08.133

Chen, W., Lu, Z., Xiao, B., Gu, P., Yao, W., Xing, J., Asiri, A. M., Alamry, K. A., Wang, X., & Wang, S. (2019). Enhanced removal of lead ions from aqueous solution by iron oxide nanomaterials with cobalt and nickel doping. *Journal of Cleaner Production*, *211*, 1250–1258. https://doi.org/10.1016/j.jclepro.2018.11.254

Dargahi, A., Golestanifar, H., Darvishi, P., Karami, A., Hasan, S. H., Poormohammadi, A., & Behzadnia, A. (2016). An investigation and comparison of removing heavy metals (lead and chromium) from aqueous solutions using magnesium oxide nanoparticles. *Polish Journal of Environmental Studies*, *25*(2), 557–562. https://doi.org/10.15244/pjoes/60281

Das, M. P., & Rebecca, L. J. (2018). Removal of lead(II) by phyto-inspired iron oxide nanoparticles. *Nature Environment and Pollution Technology*, *17*(2), 569–574.

Fahmy, H. M., Mohamed, F. M., Marzouq, M. H., Mustafa, A. B. E.-D., Alsoudi, A. M., Ali, O. A., Mohamed, M. A., & Mahmoud, F. A. (2018). Review of green methods of iron nanoparticles synthesis and applications. *BioNanoScience*, *8*(2), 491–503. https://doi.org/10.1007/s12668-018-0516-5

Fan, S., Wang, Y., Li, Y., Tang, J., Wang, Z., Tang, J., Li, X., & Hu, K. (2017). Facile synthesis of tea waste/Fe_3O_4 nanoparticle composite for hexavalent chromium removal from aqueous solution. *RSC Advances*, *7*(13), 7576–7590. https://doi.org/10.1039/c6ra27781k

Fierro, V., Torné-Fernández, V., Montané, D., & Celzard, A. (2008). Adsorption of phenol onto activated carbons having different textural and surface properties. *Microporous and Mesoporous Materials*, *111*(1), 276–284. https://doi.org/10.1016/j.micromeso.2007.08.002

Guler, U. A. (2017). Removal of tetracycline from aqueous solutions using nanoscale zero valent iron and functional pumice modified nanoscale zero valent iron. *Journal of Environmental Engineering and Landscape Management*, *25*(3), 223–233. https://doi.org/10.3846/16486897.2016.1210156

Gunatilake, S. K. (2015). Methods of removing heavy metals from industrial wastewater. *Journal of Multidisciplinary Engineering Science Studies*, *1*(1), 12–18.

Hariani, P. L., Faizal, M., Ridwan, R., Marsi, M., & Setiabudidaya, D. (2013). Synthesis and properties of Fe3O4 nanoparticles by co-precipitation method to removal procion dye. *International Journal of Environmental Science and Development*, *4*(3), 336–340. https://doi.org/10.7763/ijesd.2013.v4.366

Hasany, S. F., Ahmed, I., Rajan, J., & Rehman, A. (2012). Systematic review of the preparation techniques of iron oxide magnetic nanoparticles. *Nanoscience and Nanotechnology*, *2*(6), 148–158. https://doi.org/10.5923/j.nn.20120206.01

He, J., Xiong, D., Zhou, P., Xiao, X., Ni, F., Deng, S., Shen, F., Tian, D., Long, L., & Luo, L. (2020). A novel homogenous in-situ generated ferrihydrite nanoparticles/polyethersulfone composite membrane for removal of lead from water: Development, characterization, performance and mechanism. *Chemical Engineering Journal*, *393*, 124696. https://doi.org/10.1016/j.cej.2020.124696

Herlekar, M., Barve, S., & Kumar, R. (2014). Plant-mediated green synthesis of iron nanoparticles. *Journal of Nanoparticles*, *2014*, 1–9. https://doi.org/10.1155/2014/140614

Huang, L., Weng, X., Chen, Z., Megharaj, M., & Naidu, R. (2014). Green synthesis of iron nanoparticles by various tea extracts: Comparative study of the reactivity. *Spectrochimica Acta Part A: Molecular and Biomolecular Spectroscopy*, *130*, 295–301. https://doi.org/10.1016/j.saa.2014.04.037

Ihsanullah, Abbas, A., Al-Amer, A. M., Laoui, T., Al-Marri, M. J., Nasser, M. S., Khraisheh, M., & Atieh, M. A. (2016). Heavy metal removal from aqueous solution by advanced carbon nanotubes: Critical review of adsorption applications. *Separation and Purification Technology*, *157*, 141–161. https://doi.org/10.1016/j.seppur.2015.11.039

Jafarinejad, S., Faraji, M., Jafari, P., & Mokhtari-Aliabad, J. (2017). Removal of lead ions from aqueous solutions using novel-modified magnetic nanoparticles: optimization, isotherm, and kinetics studies. *Desalination and Water Treatment*, *92*, 267–274. https://doi.org/10.5004/dwt.2017.21562

Jumina, Priastomo, Y., Setiawan, H. R., Mutmainah, Kurniawan, Y. S., & Ohto, K. (2020). Simultaneous removal of lead(II), chromium(III), and copper(II) heavy metal ions through an adsorption process using C-phenylcalix[4]pyrogallolarene material. *Journal of Environmental Chemical Engineering*, *8*(4), 103971. https://doi.org/10.1016/j.jece.2020.103971

Kamilya, T., Mondal, S., & Saha, R. (2021). Effect of magnetic field on the removal of copper from aqueous solution using activated carbon derived from rice husk. *Environmental Science and Pollution Research*, *29*, 20017–20034. https://doi.org/10.1007/s11356-020-12158-0

Kataria, N., & Garg, V. K. (2018). Green synthesis of Fe_3O_4 nanoparticles loaded sawdust carbon for cadmium (II) removal from water: Regeneration and mechanism. *Chemosphere*, *208*, 818–828. https://doi.org/10.1016/j.chemosphere.2018.06.022

Kumar, R., & Mondal, S. (2020). Removal of fluoride from aqueous solution using coal-coated with $FeCl_3$. In A. S. Kalamdhad (Ed.), *Recent developments in waste management* (pp. 417–434). Springer. https://doi.org/10.1007/978-981-15-0990-2_34

Liu, X., Hu, Q., Fang, Z., Zhang, X., & Zhang, B. (2009). Magnetic chitosan nanocomposites: A useful recyclable tool for heavy metal ion removal. *Langmuir*, *25*(1), 3–8. https://doi.org/10.1021/la802754t

Mahurpawar, M. (2015). Effects of heavy metals on human health. *International Journal of Research -GRANTHAALAYAH*, *3*(9SE), 1–7. https://doi.org/10.29121/granthaalayah.v3.i9se.2015.3282

Martínez-Cabanas, M., López-García, M., Barriada, J. L., Herrero, R., & Sastre de Vicente, M. E. (2016). Green synthesis of iron oxide nanoparticles. Development of magnetic hybrid materials for efficient As(V) removal. *Chemical Engineering Journal*, *301*, 83–91. https://doi.org/10.1016/j.cej.2016.04.149

Moattari, R. M., Rahimi, S., Rajabi, L., Derakhshan, A. A., & Keyhani, M. (2015). Statistical investigation of lead removal with various functionalized carboxylate ferroxane nanoparticles. *Journal of Hazardous Materials*, *283*, 276–291. https://doi.org/10.1016/j.jhazmat.2014.08.025

Mondal, S., & Mahanta, C. (2017). Evaluation of arsenic adsorption capacity of indigenous materials for their suitability as filter media. *Desalination and Water Treatment*, *84*, 309–323. https://doi.org/10.5004/dwt.2017.21188

Moradi, G., Dabirian, F., Mohammadi, P., Rajabi, L., Babaei, M., & Shiri, N. (2018). Electrospun fumarate ferroxane/polyacry-

lonitrile nanocomposite nanofibers adsorbent for lead removal from aqueous solution: Characterization and process optimization by response surface methodology. *Chemical Engineering Research and Design*, *129*, 182–196. https://doi.org/10.1016/j.cherd.2017.09.022

Nassar, N. N. (2010). Rapid removal and recovery of Pb(II) from wastewater by magnetic nanoadsorbents. *Journal of Hazardous Materials*, *184*(1), 538–546. https://doi.org/10.1016/j.jhazmat.2010.08.069

Neyaz, N., Siddiqui, W. A., & Nair, K. K. (2014). Application of surface functionalized iron oxide nanomaterials as a nanosorbents in extraction of toxic heavy metals from ground water: A review. *International Journal of Environmental Sciences*, *4*(4), 472–483.

Prathna, T. C., Sharma, S. K., & Kennedy, M. (2017). Development of iron oxide nanoparticle adsorbents for arsenic and fluoride removal. *Desalination and Water Treatment*, *67*, 187–195. https://doi.org/10.5004/dwt.2017.20464

Rajput, S., Pittman, C. U., & Mohan, D. (2016). Magnetic magnetite (Fe_3O_4) nanoparticle synthesis and applications for lead (Pb^2+) and chromium (Cr^6+) removal from water. *Journal of Colloid and Interface Science*, *468*, 334–346. https://doi.org/10.1016/j.jcis.2015.12.008

Saleh, T. A., Tuzen, M., & Sarı, A. (2017). Magnetic activated carbon loaded with tungsten oxide nanoparticles for aluminum removal from waters. *Journal of Environmental Chemical Engineering*, *5*(3), 2853–2860. https://doi.org/10.1016/j.jece.2017.05.038

Sarkar, Z. K., & Sarkar, F. K. (2013). Selective removal of lead (II) ion from wastewater using superparamagnetic monodispersed iron oxide (Fe_3O_4) nanoparticles as a effective adsorbent. *International Journal of Nanoscience and Nanotechnology*, *9*(2), 109–114.

Shi, Z., Xu, C., Guan, H., Li, L., Fan, L., Wang, Y., Liu, L., Meng, Q., & Zhang, R. (2018). Magnetic metal organic frameworks (MOFs) composite for removal of lead and malachite green in wastewater. *Colloids and Surfaces A: Physicochemical and Engineering Aspects*, *539*, 382–390. https://doi.org/10.1016/j.colsurfa.2017.12.043

Sulistyaningsih, T., Santosa, S. J., Siswanta, D., & Rusdiarso, B. (2017). Synthesis and characterization of magnetites obtained from mechanically and sonochemically assissted co-precipitation and reverse co-precipitation methods. *International Journal of Materials, Mechanics and Manufacturing*, *5*(1), 16–19. https://doi.org/10.18178/ijmmm.2017.5.1.280

Wu, W., He, Q., & Jiang, C. (2008). Magnetic iron oxide nanoparticles: Synthesis and surface functionalization strategies. *Nanoscale Research Letters*, *3*(11), 397. https://doi.org/10.1007/s11671-008-9174-9

Xu, P., Zeng, G. M., Huang, D. L., Lai, C., Zhao, M. H., Wei, Z., Li, N. J., Huang, C., & Xie, G. X. (2012). Adsorption of Pb(II) by iron oxide nanoparticles immobilized Phanerochaete chrysosporium: Equilibrium, kinetic, thermodynamic and mechanisms analysis. *Chemical Engineering Journal*, *203*, 423–431. https://doi.org/10.1016/j.cej.2012.07.048

Yew, Y. P., Shameli, K., Miyake, M., Ahmad Khairudin, N. B. B., Mohamad, S. E. B., Naiki, T., & Lee, K. X. (2020). Green biosynthesis of superparamagnetic magnetite Fe_3O_4 nanoparticles and biomedical applications in targeted anticancer drug delivery system: A review. *Arabian Journal of Chemistry*, *13*(1), 2287–2308. https://doi.org/10.1016/j.arabjc.2018.04.013

Zeng, X., Chen, Q., Tan, Q., Xu, H., Li, W., Yang, S., Wang, J., Ren, J., Luo, F., Tang, J., Wu, L., Zhang, Y., & Liu, D. (2021). Risk assessment of heavy metals in soils contaminated by smelting waste for the perspective of chemical fraction and spatial distribution. *Journal of Environmental Engineering and Landscape Management*, *29*(2), 101–110. https://doi.org/10.3846/jeelm.2021.14190

Zhu, Y., Hu, J., & Wang, J. (2012). Competitive adsorption of Pb(II), Cu(II) and Zn(II) onto xanthate-modified magnetic chitosan. *Journal of Hazardous Materials*, *221–222*, 155–161. https://doi.org/10.1016/j.jhazmat.2012.04.026